Optical Model Studies of the Salt-Induced 10–30-nm Fiber Transition in Chromatin†

Rodney E. Harrington
Department of Biochemistry, University of Nevada, Reno, Reno, Nevada 89557-0014
Received July 2, 1984; Revised Manuscript Received October 17, 1984

ABSTRACT: Fractionated chicken erythrocyte chromatin fibers consisting of 10-mer and 75-mer polynucleosomes have been studied by flow birefringence and viscosity over a range of Na^+ and Mg^{2+} ion concentrations sufficient to span the 10–30-nm fiber transition. Negative intrinsic flow bifringence was observed under all solvent conditions investigated. The intrinsic birefringence, obtained from the reduced birefringence to intrinsic viscosity ratio, was used to evaluate various optical models for the DNA conformation in the fiber. Results are consistent with an extended chromatosome-linker "necklace" model for the unfolded, low-salt fiber and with a solenoidal model of edge-stacked chromatosomes for the condensed fiber at high salts. These results are consistent with and independently corroborative of similar models based upon electric dichroism and neutron scattering reported by others.

The structure of chromatin is now believed to consist of a hierarchy of different levels of coiling. The lowest level, the nucleosome, packages DNA with a packing ratio of about 7 to 1 and has been extensively characterized by using a wide variety of structural methods. Although its crystallographic structure is just now being determined to atomic resolution (Richmond et al., 1984), results from other studies strongly suggest that is consists of 168 base pairs (bp) of DNA wound in two left-handed superhelical turns about an octamer of core histones ($H2A_2$, $H2B_2$, $H3_2$, and $H4_2$) plus interparticle "linker" DNA whose length depends upon the chromatin source and ranges from approximately zero (yeast) to 73 bp (sea urchin sperm) (Kornberg, 1977). Subunits of the nucleosome which have also been well characterized are the 144 bp "core particle", a subunit of unusual stability to enzymatic degradation, and the 168 bp "chromatosome" stabilized by histone H1 binding at or near the DNA termini. These sublevels of chromatin structure have been extensively reviewed (McGhee & Felsenfeld, 1980; Mirzabekov, 1980).

It is now generally accepted that the chromatosome plus linker DNA constitutes the basic unit of assembly for the next higher orders of chromatin structure (Simpson, 1978; Thoma et al., 1979). At very low ionic strength conditions (and in the absence of polyvalent ions), the chromatosome-linker "copolymer" forms a relatively flexible fiber approximately 10 nm in diameter (Thoma et al., 1979; Finch & Klug, 1976; Ris & Korenberg, 1979; Ruiz-Carillo et al., 1980; Finch et al., 1977). At higher ionic strengths, and particularly in the presence of divalent cations, this fiber condenses into a more compact configuration approximately 30 nm in diameter (Thoma et al., 1979; Finch & Klug, 1976; Ris & Korenberg, 1979). It has been suggested from electron microscopy (Thoma et al., 1979; Finch & Klug, 1976), neutron scattering (Baldwin et al., 1978; Suau et al., 1979), and X-ray diffraction (Azorin et al., 1980) studies that this fiber is solenoidal with a pitch of 11 nm and six nucleosomes per turn. However, the precise details of chromatosome orientation within the 10- and 30-nm fibers are still somewhat controversial, due in part to the extreme difficulty of characterizing structurally these complex systems in solution or interpreting electron microscope visualizations and extrapolating them to these conditions.

Solution optical methods, e.g., electric and linear flow dichroism and birefringence, have proved useful and in some respects are unique methods for elucidating the structures of the 10- and 30-nm fibers in higher order chromatin (Houssier & Fredericq, 1966; Colson et al., 1974; Rill & Van Holde, 1974; Marion & Roux, 1978; Edmonds-Alt et al., 1979; Houssier & Tricot, 1979; Roux et al., 1979; McGhee et al., 1980, 1983; Houssier, 1981; Houssier et al., 1981a,b; Lee et al., 1981; Tjerneld et al., 1982; Harrington, 1983; Makarov et al., 1983; Matsuoka et al., 1984) and in characterizing the transitions between them (McGhee et al., 1980, 1983; Lee et al., 1981; Tjerneld et al., 1982; Harrington, 1983; Makarov et al., 1983; Matsuoka et al., 1984). DNA in the B family of structures has its base planes approximately perpendicular to the overall helical axis. The π-electron clouds of the purines and pyrimidines are highly polarizable, and hence, the optical anisotropy factor in the birefringence is large. This leads to a large, negative birefringence in DNA. For an oriented system of DNA-containing structures, therefore, the intrinsic birefringence is usually an extremely sensitive function of DNA trajectory, and much structural information can be obtained from a compaison of the experimental birefringence to that deduced from appropriate (optical) models. The intense electronic transitions observed in the purine and pyrimidine bases at about 260 nm are a π to π^* transition involving bonding π orbitals between C and N atoms (Kasha et al., 1961). Its transition momenet is relatively large and is parallel to the base plane. Thus, the dichroism is also large and negative at this wavelength, and experimental dichroism on oriented DNA-containing systems is similarly interpretable in structural terms. Form effects are present in both types of experiments. These effects are not well understood and are generally described in terms of classical (macroscopic continuum dielectric) optical theory (Fredericq & Houssier, 1973). The form effect in birefringence is always positive for prolate particles and negative for disks. The dichroism form effect is positive when the particle refractive index is greater than that of the solvent (the usual case on the long wavelength side of the absorption band) and negative when it is less. In both cases, the form effect vanishes when the particle refractive

† This research was supported by National Science Foundation Research Grant PCM 7905609, by National Institutes of Health Research Grant R01 GM33435, and by the Agricultural Experiment Station of the University of Nevada, Reno, through Hatch Project 131.

0006-2960/85/0424-2011$01.50/0

index equals that of the surrounding solvent. The classical treatment of form birefringence has been criticized in the case of proteins and is believed to overestimate seriously the effect for these systems (Taylor & Cramer, 1963; Oriel & Schellman, 1966; Fredericq & Houssier, 1973). Since the form effect in dichroism is numerically smaller, this is usually considered an advantage in this type of measurement.

In my laboratory, flow birefringence can be measured with considerable precision and sensitivity. Hence, I have emphasized birefringence and its interpretation in spite of the form effect problem. It has been shown in DNA that the form birefringence models very nearly in the same way as the intrinsic birefringence [see Harrington (1979, 1982) and references cited therein]. Thus, it is reasonable to compare the effective intrinsic birefringence of a DNA-containing system such as chromatin calculated by using macroscopic dielectric theory to that for various models of DNA trajectories based upon the experimental intrinsic birefringence of pure DNA measured and calculated in the same way. Such a relative use of the classical theory alleviates the problem of possible errors in partitioning the total observed birefringence into its intrinsic and form components.

In the present work, I present results of flow birefringence/intrinsic viscosity studies on fractionated 10-mer and 75-mer polynucleosome systems. Flow methods of particle orientation offer some advantages over electric field orientation. The theory of hydrodynamic orientation is well understood for rigid particles and flexible chain systems, and considerable evidence exists that is it rigorous (Harrington, 1967, 1970a,b). In contrast, high-field electrical studies may be complicated by effects associated with induction and ion atmosphere migration. Such effects are not yet well understood. Also, electrical orientation studies are necessarily limited to solutions of relatively low conductivity, although this problem can be alleviated somewhat by careful apparatus design. Perhaps the most important difference between the present work and other optical studies on chromatin is that measurement of optical anisotropy is made in the limit of zero particle perturbation (zero shear) and concentration. This is made possible by the high level of sensitivity currently available in flow birefringence measurements. The equivalent electrical experiments require extrapolation to infinitely high field, and in linear flow dichroism studies reported to date, the orientation factor is assumed to be known and the particles are assumed to be hydrodynamically unperturbed under the relatively high shear conditions at which the experiments are conducted.

The systems studied were taken through the 10–30-nm fiber transition by titrating with Na^+ or Mg^{2+} ion. In all cases, the unfolded (low-salt) form of the fiber showed a strong negative flow birefringence. The folded (high-salt) form showed a weak positive birefringence. This change in sign of the birefringence is entirely attributable to the form effect. Results of this study are in semiquantitative agreement with the electric dichroism studies of McGhee et al. (1980, 1983) and agree in algebraic sign of the optical effect at low ionic strength with linear flow dichroism studies on similar chromatin preparations (Walter Baase, private communication). However, some discrepancies exist between this work and certain other linear flow dichroism studies on other chromatin systems (Tjerneld et al., 1982; Makarov et al., 1983; Matsuoka et al., 1984). The exact reasons for these discrepancies are not yet clear.

Background on the Theory of Flow Birefringence

The theory of flow birefringence relevant to this work has been discussed in detail elsewhere (Harrington, 1967, 1970a,b, 1979, 1981, 1982). Only a brief outline will be presented here.

The ratio of the reduced Maxwell coefficient, $[n] = (\Delta n/cG\eta_0)_{c,G\to 0}$, to the intrinsic viscosity, $[\eta] = (\ln \eta_{rel}/c)_{c,G\to 0}$, where Δn is the flow birefringence, c is the weight concentration, G is the velocity gradient in s^{-1}, η_0 is the absolute solvent viscosity, and η_{rel} is the relative viscosity of solution, is independent of the hydrodynamic model and is a function only of the optical anisotropy (Harrington, 1967, 1970a,b):

$$\frac{[n]}{[\eta]} = \frac{4\pi\bar{v}M_r d}{5nRT}(g_a - g_b) \tag{1}$$

In eq 1, $\bar{v}$ is the partial specific volume, M_r is the relative molecular weight, d is a function of the shape (axial ratio) of a rigid solute particle, n is the refractive index of solution, R is the molar Boltzmann constant, T is the absolute temperature, and the optical terms g_i are particle shape dependent functions of refractive index components along the indicated particle axes.

For particles of ellipsoidal or cylindrical symmetry, the g_i values are also functions of the refractive index increment

$$\frac{dn}{dc} = \frac{2\pi\bar{v}}{3n}(g_a + 2g_b) \tag{2}$$

where subscript a refers to the major axis and b to the minor axes of elliptical or cylindical particles. Equations 1 and 2 allow g_i to be obtained independently from experimental values of $[n]/[\eta]$, dn/dc, $\bar{v}$, and n. Because of the particle shape dependence of various quantitites in eq 1 and 2, the g_i values so obtained are also functions of particle shape anisometry.

The optical anisotropy $(g_a - g_b)$ from eq 1 contains both the intrinsic and form contributions to the flow birefringence. To obtain the intrinsic birefringence, $\Delta n_{int} = (n_a - n_b)$, and hence the n_i, the form contribution to $g_a - g_b$ must be explicitly considered. The theory of continuum macroscopic dielectrics has been used to estimate the form effect (Fredericq & Houssier, 1973; Peterlin & Stuart, 1939) using the early treatment of Wiener. The result applicable to rods and disks is

$$4\pi g_i = \frac{n_i^2 - n_0^2}{1 + [(n_i^2 - n_0^2)/n_0^2]L_i} \tag{3}$$

where n_i is the ith component of the particle refractive index and the subscript 0 refers to pure solvent. The L_i values are inner field shape factors which can be approximated for ellipsoids and cylinders (Harrington, 1970a,b, 1981). Equation 3 can be extended to particles of ellipsoidal symmetry by employing the (axial ratio dependent) Peterlin & Stuart (1939) values of L_i. Within this theoretical framework, eq 1–3 can be used to estimate the principal refractive index components, n_i, as functions of particle shape anisometry from experimental $[n]/[\eta]$, dn/dc, and $\bar{v}$ data. The major weakness of this procedure is the classical optical treatment for the form birefringence, eq 3.

The intrinsic birefringence of a given DNA trajectory can be obtained from a tensoral summation of polarizability per volume components (γ_i) of pure DNA by using the relationship

$$n_i^2 = 1 + 4\pi\gamma_i \tag{4}$$

The principal γ_i components for the DNA helix have been determined from flow birefringence and intrinsic viscosity data on short, rigid persistence length DNA fragments by using the considerations developed above (Sarquis & Harrington, 1969; Harrington, 1970b). The results (Harrington, 1970b) are the following: $n_a = 1.6222$ and $n_b = 1.7490$ so that $\Delta n_{int} = n_a -$

$n_b = -0.1268$. An assumption implicit in this type of optical trajectory analysis is that the DNA is the principal determinant of the particle birefringence and that any associated proteins contribute negligibly to the optical anisotropy. This assumption seems justified and has been discussed elsewhere (Harrington, 1981, 1982).

Two additional considerations must be kept in mind in optical DNA trajectory analyses based upon flow birefringence. The first involves the form birefringence and its classical treatment just discussed. Applicability of the classical theory has been criticized by several investigators (Taylor & Cramer, 1963; Oriel & Schellman, 1966) at least in the case of proteins. The failure of eq 3 to partition correctly the intrinsic and form birefringence is ascribed to that fact that the particles are too small for macroscopic continuum dielectric theory strictly to apply, yet are large with respect to the wavelength of the incident light (Oriel & Schellman, 1966). On the other hand, considerable evidence exists that macroscopic continuum dielectric theory is quite satisfactory at the molecular level for many systems (Harrington, 1967, 1970b). Discrepancies of this type cancel to a considerable extent in optical trajectory analyses since the optical parameters for the pure DNA used in the optical models are also derived from flow birefringence and are obtained by using the same classical theory (Harrington, 1970b). This will be especially true if particle size is the principal problem. A second and potentially more serious problem arises from uncertainties in the hydrodynamic orientation of the particles in a shear field. Since the nature of the hydrodynamic orientation of oblate- and prolate-shaped particles in a velocity gradient is conceptually different, an a priori assumption as to the general particle shape is required. However, this type of information is often available from the extinction angle, from an independent determination of the rotational diffusion constant, or from other conformationally sensitive biophysical measurements.

Experimental Procedures

Chromatin was prepared from chicken erythrocytes following as closely as possible the protocols of McGhee et al. (1980) and of Shinde et al. (1980). Micrococcal nuclease digestion was stopped by adding ethylenediaminetetraacetic acid (EDTA) to 5 mM. The cooled digest was then pelleted at 1000*g* for 6 min, resuspended in 0.25 mM EDTA, and centrifuged at 8000*g* for 30 min to remove cellular debris. The resulting soluble chromatin preparation was then run on isokinetic sucrose gradients containing 5 mM tris(hydroxymethyl)aminomethane hydrochloride (Tris-HCl) and 0.1 mM EDTA at pH 8, and fractions corresponding to ~10-mer and ~75-mer polynucleosomes (as determined by DNA length) were collected, pooled, and dialyzed to equilibrium against a 0.22 mM cacodylic acid, 0.2 mM NaOH, and 0.005 mM EDTA, pH 7, buffer. This procedure resulted in ~10% total DNA recovery. Scans of 0.6% agarose sizing gels for the two pooled fractions are shown in Figure 1. Size markers were *Hin*dIII digests of λ phage DNA. Histone bands from the unfractionated chromatin preparations on 18% polyacrylamide–sodium dodecyl sulfate ($NaDodSO_4$) gels showed all five core histones present in normal density bands (data not shown).

The gel tracings of Figure 1 were obtained by using an EC Apparatus Co. EC 910 transmission densitometer. The output was digitized into 500 point files using a Nelson Analytical 760 A/D converter interfaced to a Hewlett-Packard 85B microcomputer. The data were computer smoothed by using a running least-squares five-point linear Chebyshev polynomial algorithm and were plotted on an HP 7225A plotter by using

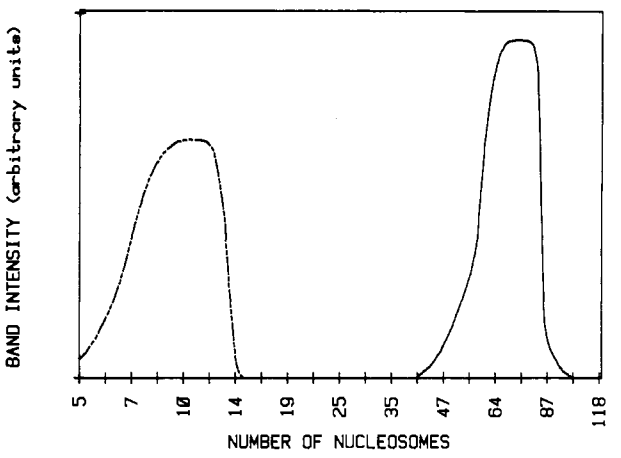

FIGURE 1: Tracings of 0.6% agarose DNA sizing gels for the 10-mer (-··-) and 75-mer (—) chicken erythrocyte chromatin preparations fractionated as described in the text. Nucleosome numbers were determined against *Hin*dIII digests of λ phage DNA size markers. Band intensity data were computer processed as discussed in the text.

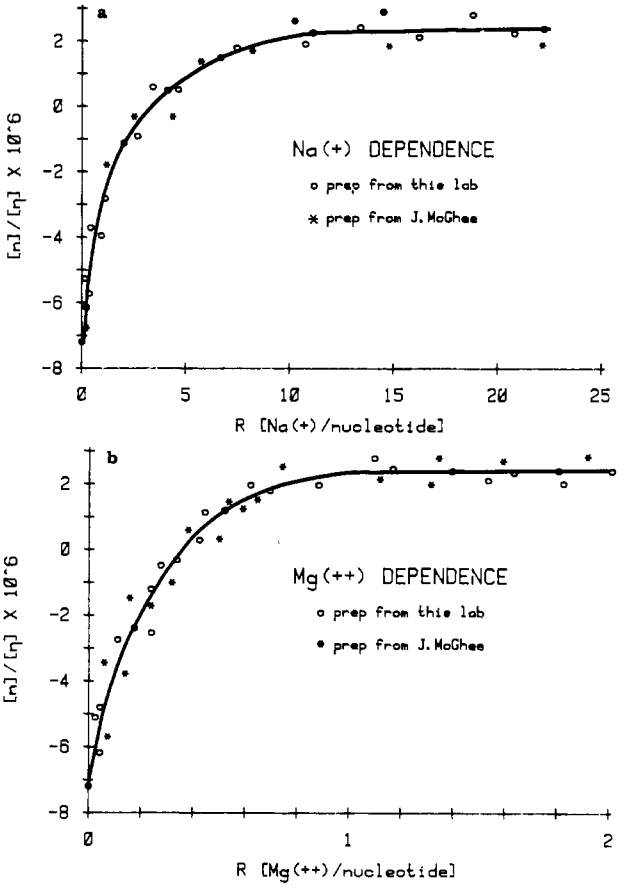

FIGURE 2: Dependence of the ratio of reduced birefringence to intrinsic viscosity, $[n]/[\eta]$, or degree of folding in the 75-mer fractionated chromatin sample as a function of (a) Na^+ and (b) Mg^{2+} ion concentration. (*) Comparison data on a chicken erythrocyte chromatin sample obtained as a gift from Dr. J. D. McGhee (see text).

an algorithm connecting data points by a running, best-fit parabola. These application programs written in HP Basic are available upon request.

A second unfractionated preparation was received as a gift from Dr. J. D. McGhee (Laboratory of Molecular Biology, NIADDK, National Institutes of Health, Bethesda, MD)[1] and

[1] Present address: Department of Medical Biochemistry, School of Medicine, University of Calgary, Calgary, Alberta, Canada T2N 1N4.

was fractionated on an isokinetic sucrose gradient as just described. A peak corresponding to ~75-mer polynucleosomes somewhat broader than that described above was collected, dialyzed into the 0.22 mM cacodylic acid buffer, and run in comparative fashion with the 75-mer fractions prepared in my laboratory (see Figure 2).

Optical Anisotropy Measurements. Flow birefringence data were obtained by using a special photoelectric scanning instrument developed and constructed in this laboratory. Details of the instrument and general protocols for its operation have been given elsewhere (Harrington, 1970b, 1979; Barrett & Harrington, 1977). A thermostated stainless-steel concentric cylinder flow cell with a rotating outer cylinder was used for all determinations. The optical path was 10 cm and the annular gap 0.23 mm; with this cell, determinations could be made on ~1–1.5-mL samples. Previous tests with this cell using a 0.5-mm gap inner cylinder suggested that its effective upper limit for laminar shear was >17 000 s^{-1} (Harrington, 1981). No evidence for turbulence at the shear rates reported here was observed. Data were collected and processed on an interfaced Hewlett-Packard 85A microcomputer using software developed by the author for this purpose on the basis of the data reduction method of Barrett & Harrington (1977). At velocity gradients >1000 s^{-1}, data were collected during 15-s flow cell run periods followed by 5 min of thermal reequilibration with the flow cell at rest. Under these conditions, negligible sample heating occurred under any experimental conditions reported here, and optical noise deriving from thermal fluctuations in the flow cell was substantially reduced. As in previous runs, averages of both senses of flow cell rotation were used to eliminate interaction between flow cell rotation and the optical scanning system (Harrington, 1979). Data were taken at pairs of the scanning system angular orientations chosen to maximize sensitivity to extinction angle measurement (Harrington, 1970c, 1979).

Intrinsic viscosity was determined by using a Cartesian diver rotational viscometer. Details of the instrument have been reported elsewhere (Gill & Thompson, 1967; Harrington & Martin, 1969). Determination of intrinsic viscosity could be made on ~0.7-mL samples to about 3% precision by using the materials in this sudy.

Studies of the 10–30-nm Fiber Transition. Fresh chromatin samples were diluted with stock buffer containing Na^+ or Mg^{2+} to the desired total ionic concentration. These were then used directly in the flow birefringence instrument or viscometer. Samples for flow birefringence were centrifuged immediately prior to use to remove particulate matter. All samples for concentration dependence of flow birefringence or viscosity were prepared from fresh chromatin stock as noted above. Hence, all data were obtained on each sample in less than 2 h, and for flow birefringence usually considerably less than this. All experimental data were taken at 15 °C. Glass-distilled water was used for all preparations. The refractive index increment (dn/dc) and the partial specific volume ($\bar{v}$) were taken as previously reported for nucleosomes (Harrington, 1981, 1982).

It is of special significance that the present data were collected within a short time following up-titration of the samples in ionic strength since a slow and apparently irreversible change in the chromatin was observed after a period of 3–6 h at ionic strengths greater than ~1 mM Na^+ (R in Figure 2a of ~0.2). This change was always in the direction of numerically increasing flow birefringence and after several hours occasionally led to a sign inversion from negative to positive. Similar observations on similar chromatin preparations have been observed by others (Walter Baase, private communication). The rate of this change was slowed significantly at reduced temperatures and at low concentrations, and the effect seemed to be less significant for Mg^{2+} at equivalent R values (Figure 2b) than for Na^+. In my hands, this change was not quantitatively reproducible, and I have simply circumvented it by ensuring that all measurements were completed within the initial induction period. I attribute these observations to a slow nonspecific aggregation of the chromatin, especially since the flow birefringence changes also were accompanied by a measurable increase in the intrinsic viscosity.

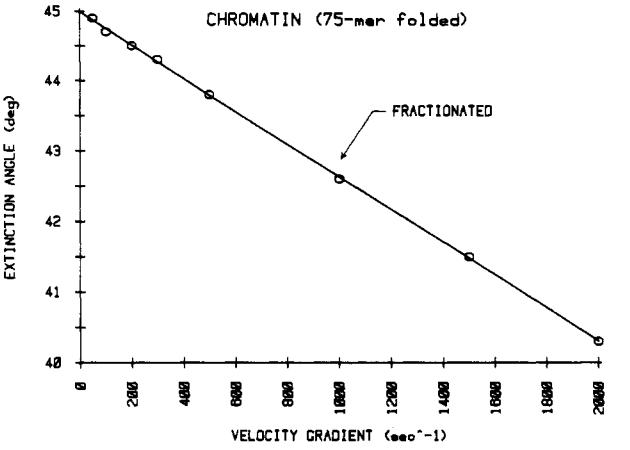

FIGURE 3: Extinction angles extrapolated to zero concentration vs. velocity gradient for the 75-mer chromatin fiber fraction at high salt concentration.

RESULTS

Chromatin fractions containing approximately 10-mer and 75-mer polynucleosome sizes were used because these were significantly represented in the size distributions of prepared chromatin. However, these sizes are suitable for characterization of the unfolded and folded states, respectively. Unfolded chromatin fragments larger than ~10-mers show flexibility and hence are difficult to characterize by optical model analysis, while folded fragments shorter than ~75-mers are rigid but relatively isometric. DNA gel scans for fractionated systems in this work, calibrated in chromatosome lengths, are shown in Figure 1.

The 10–30-nm fiber transition (unfolded to folded state) was studied by increasing either Na^+ or Mg^{2+} ion concentrations. Results for the 75-mer fraction are shown in panels a and b, respectively, of Figure 2. The state denoted "unfolded" in subsequent discussion lies at the bottom of these curves, i.e., 0.2 mM Na^+, and 0.005 mM EDTA, pH 7, and the "folded" state is taken from the plateau region of Figure 2 at 75 mM Na^+ (R = 16.5). The transitions were identical within experimental error for the 10-mer fractions (data not shown), and hence the same limiting definitions apply to this case also.

Experimental results for the folded 75-mer are shown in Figures 3 and 4. The extinction angle data of Figure 3 correspond to a rotational diffusion coefficient (D_r) of 2×10^3 s^{-1} for a rigid prolate particle (Harrington, 1979, 1981). This is consistent with the physical dimensions and axial ratio $p \simeq 5$ of a cylinder ~30 nm in diameter and ~140 nm in length according to the hydrodynamic equations of Tirado & Garcia de la Torre (1980). The curve of Figure 3 lies almost on the theoretical curve for a rigid prolate ellipsoid (Peterlin & Stuart, 1939), suggesting that the folded 75-mer is hydrodynamically a rigid assembly. This is in agreement with McGhee et al.

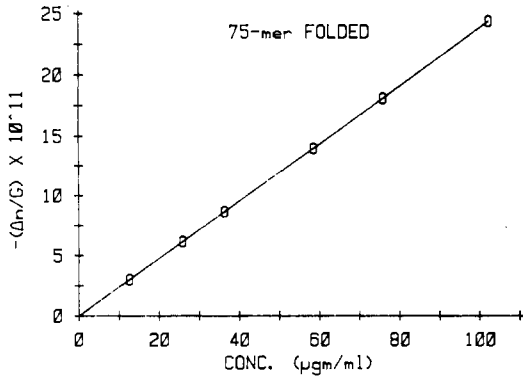

FIGURE 4: Concentration dependence of $(\Delta n/G)_{G\to 0}$ for the fractionated 75-mer chromatin fiber at high salt concentration.

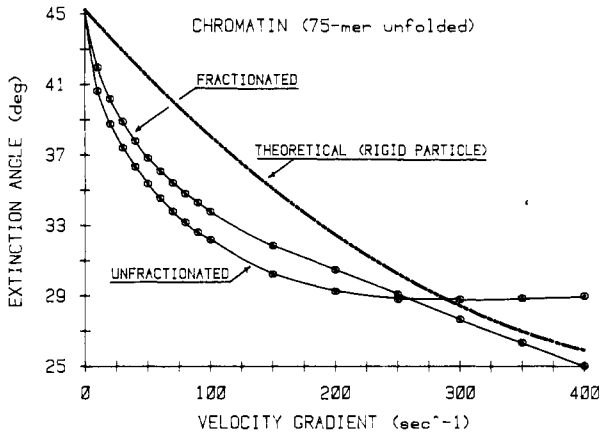

FIGURE 5: Extinction angles extrapolated to zero concentration vs. velocity gradient for the fractionated 75-mer chromatin fiber at low salt concentration compared to unfractionated chromatin from the same preparation at low salt concentration. The dashed line is the theoretical curve for a hypothetical rigid 75-mer particle (see text).

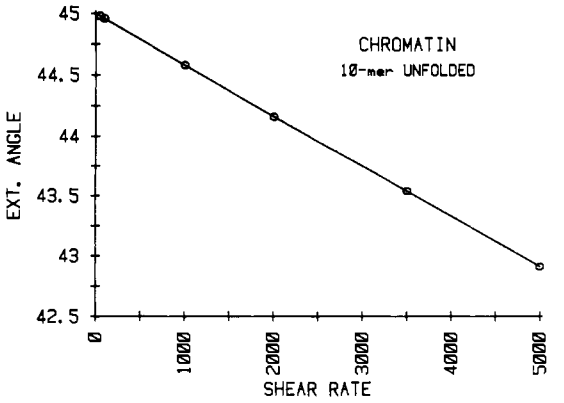

FIGURE 6: Extinction angles extrapolated to zero concentration vs. velocity gradient for the 10-mer chromatin fiber fraction at low salt concentrations. Extinction angles in degrees and velocity gradient in s^{-1}.

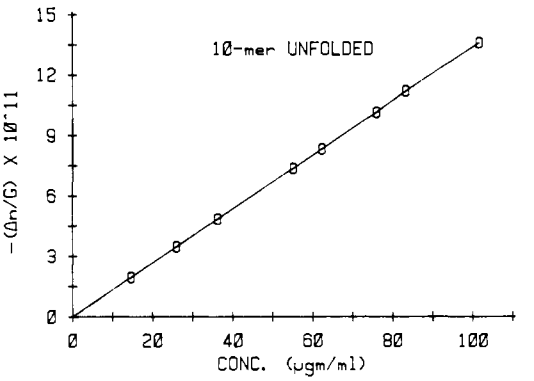

FIGURE 7: Concentration dependence of $(\Delta n/G)_{G\to 0}$ for the fractionated 10-mer chromatin fiber at low salt concentration.

(1980, 1983), who used electric dichroism to determine rotational relaxation times for ~45-mer fibers and concluded from the absence of higher relaxation times that these particles were hydrodynamically rigid. The flow birefringence vs. shear curves at all concentrations studied were essentially linear (data not shown). The concentration dependence $(\Delta n/G)_{G\to 0}$ in Figure 4 is obtained from their limiting slopes. The high degree of linearity in the shear curves is also suggestive of hydrodynamic rigidity in the particles.

The unfolded (10-nm fiber) form of the 75-mer shows evidence of significant flexibility, again in qualitative agreement with the studies of McGhee et al. (1980, 1983). The shear dependence of the birefringence is nonlinear throughout the low-shear range (data not shown), and hence, these data cannot be interpreted in a straightforward way by using optical model analysis. Associating this nonlinearity with particle flexibility is suggested by the extinction angle vs. shear data shown in Figure 5. The extinction angle curve for the fractionated 75-mer shows considerable curvature, even at relatively low-velocity gradients. This curve is actually qualitatively similar to that obtained for semiflexible chain macromolecules (Harrington, 1967) or for DNA of considerably higher molecular weight (Harrington, 1970b; Sarquis & Harrington, 1969). For comparison, the theoretical extinction angle curve for an equivalent rigid cylinder is also shown in Figure 5. This cylinder is taken to have a rotational diffusion constant of 70 s^{-1} so that its extinction angle roughly corresponds to the experimental value for the fractionated 75-mer at the highest shear rate reported (400 s^{-1}). Assuming a diameter of 11 nm, this corresponds to a cylinder axial length of ~500 nm (Tirado & Garcia de la Torre, 1980) or roughly half the ~1050-nm length calculated for the linker DNA of a 75-mer polynucleosome assumed extended along a common axis. (A rigid cylinder of 1050-nm axial length and 11-nm diameter would have $D_r \simeq 20$ s^{-1} and would be almost completely oriented in a shear field of 400 s^{-1}.

The effect of polydispersity upon extinction angle data is also shown in Figure 5. Inflection of extinction angle curves with shear is characteristic of anisometric systems with significant polydispersity and illustrates the sensitivity of extinction angle measurements to a distribution in particle lengths (Scheraga & Signer, 1960; Harrington, 1967). Because the contributions of the various size increments to the extinction angle are not linearly additive (Scheraga & Signer, 1960; Harrington, 1967), the contribution of each particle to the observed extinction angle is different at different regions of the shear curve. These considerations apply equally to rigid or flexible particles and to chain macromolecules. In fact, if the particle size distribution is Gaussian, it can be shown (Scheraga, 1951; Scheraga & Signer, 1960) that the limiting low-shear end of the curve approaches that of the largest or most orientable particles in the sample. At higher gradients, shorter particles make increasingly greater contributions until the limiting high-shear region becomes characteristic of the average of all particles. Thus, the extinction angle vs. shear curves which have been reported for highly polydisperse samples to contain sigmoidal inflections can be explained, and the curves themselves can yield semiquantitative information on the polydispersity itself. A hint of this type of effect is evident in the curve for the fractionated sample in Figure 5 above

200-s^{-1} shear, indicating that the residual polydispersity even in this sample is still significant with respect to the extinction angle.

Experimental results for the unfolded 10-nm fiber form of the 10-mer fraction are given in Figures 6 and 7. Although these particles must have some degree of kinetic flexibility by analogy with the longer unfolded fragments of Figure 5, their shorter overall length (~130 nm if the linker DNA is fully extended along the same axis) evidently reduces flexibility effects to below the limit of detection using present methods. The shear-dependent extinction angle curve of Figure 6 is almost linear below 5000-s^{-1} shear and is consistent with a prolate axial ratio $p \cong 10$ and a rotational diffusion constant $D_r = 1.1 \times 10^4\ s^{-1}$. This corresponds to a rigid cylinder length of 84 nm using the Tirado & Garcia de la Torre (1980) model with diameter 11 nm. If the linker DNA were fully extended, the length would be 130 nm. The discrepancy is probably due both to flexibility and to deviations of the actual shape from that of a true cylinder. The shear dependence of the flow birefringence is also essentially linear (data not shown) as is the concentration dependence of Figure 7. It is evident, therefore, that the Maxwell coefficient, $[n] = (\Delta n/cG\eta_0)_{c,G\to 0}$, determined in these experiments is the true limiting value.

The folded (high-salt) form of the 10-mer did not show appreciable orientation at velocity gradients up to 10 000 s^{-1}, and hence, the flow birefringence and particularly the extinction angles were below the level of detectability. Between 10 000 and 16 000 s^{-1} (the approximate upper limit to the laminar flow range of the flow cell used), some orientation appeared to occur, but the data were largely unrecoverable from optical noise in the flowing solution using signal averaging and enhancement technology available. Since the level of sensitivity in these experiments is comparable to that in earlier studies of pure nucleosome cores (Harrington, 1979, 1981, 1982; Harrington et al., 1982), these findings suggest that the folded 10-mer is highly isometric.

Table I: Summary of Experimental and Derived Quantities for Fractionated Chicken Erythrocyte Chromatin Fibers in Two Size Fractions, 10-mer and 75-mer Polynucleosomes

10-mn fiber	30-nm fiber
10-mer, low ionic strength (unfolded)	10-mer, high ionic strength (folded)[c]
$[\eta] = (-1.810 \pm 0.152) \times 10^{-4}$	$[n] = -2.678 \times 10^{-6}$
$[\eta] = 112\ cm^3/g$	$[\eta]$ (not available)
$[\eta]/[\eta] = -1.616 \times 10^{-6}$	$[n]/[\eta]$ (not available)
$g_1 - g_2 = -1.195 \times 10^{-2}$ [a]	
$\Delta n_{int} = -0.114$ [a]	
$M_r \simeq 2.8 \times 10^6$	
75-mer, low ionic strength (unfolded)	75-mer, high ionic strength (folded)
$[n] = -3.632 \times 10^{-3}$	$[n] = (2.653 \pm 0.015) \times 10^{-4}$
$[\eta] = 504.5\ cm^3/g$	$[\eta] = 111\ cm^3/g$
$[\eta]/[\eta] = -7.198 \times 10^{-6}$	$[n]/[\eta] = (2.390 \pm 0.013) \times 10^{-6}$
$g_1 - g_2 = -5.87 \times 10^{-3}$ [b]	$g_1 - g_2 = 4.44 \times 10^{-3}$ ($r = 3$)
$\Delta n_{int} = -8.75 \times 10^{-2}$ [b]	$g_1 - g_2 = 3.07 \times 10^{-3}$ ($r = 5$)
	$g_1 - g_2 = 2.36 \times 10^{-3}$ ($r = 10$)
	$\Delta n_{int} = -2.02 \times 10^{-2}$ ($r = 3$)
	$\Delta n_{int} = -3.64 \times 10^{-2}$ ($r = 5$)
	$\Delta n_{int} = -4.60 \times 10^{-2}$ ($r = 10$)
	$D_r \simeq 2 \times 10^3\ s^{-1}$
	$M_r = 2.1 \times 10^7$

[a] Assumed axial ratio $r \simeq 10$. [b] Assuming rigid particle conformation with prolate axial ratio $r \simeq 85$. [c] Results consistent with a particle of high symmetry and with an axial ratio near unity.

Discussion

30-nm Fiber. Two principal orientation schemes can be envisioned for the chromatosomes in the folded 30-nm fiber (Suau et al., 1979; Azorin et al., 1980; McGhee et al., 1980, 1983): a solenoid with the flat faces of the nucleosomal disk generally parallel to the solenoidal axis; a corresponding perpendicular orientation. The first of these is consistent with electrooptical (McGhee et al., 1980, 1983) and neutron scattering (Suau et al., 1979) studies and is supported by the results presented here. There appears to be no way to rationalize the hydrodynamic (extinction angle) data with a solenoidal model in which the nucleosomes are aligned principally normal to the helical axis. The optical (birefringence) data are ambiguous but are more consistent with edge stacking of the nucleosomes than with a face-stacked solenoidal model.

The absence of significant orientation for the folded 10-mer fiber requires that these particles have a high level of isometry or quasi-spherical symmetry. Given that the diameter is on the order of two nucleosome widths, this could only be true if the nucleosomes were stacked edge to edge along the helical axis. A face to face stacking would lead to an oblate particle of axial ratio <0.5 assuming the solenoidal conformation is maintained in these short fragments. From past experience with nucleosomes (Harrington, 1981, 1982), anisometry of this magnitude should be easily detected and measured in these experiments.

The extinction angle data on the 75-mer folded fragment also suggest an edge to edge configuration of nucleosomes in the solenoid. The rotational diffusion coefficient ($D_r \cong 2 \times 10^3\ s^{-1}$) obtained from the shear dependence of the extinction angle is consistent with a cylinder 30 nm in diameter and 150 nm in height (Tirado & Garcia de la Torre, 1980). These dimensions are roughly those of a helical array of edge-stacked nucleosomes having 6 nucleosomes per turn and 12–13 turns overall. If the chromatosomes were face stacked, the cylinder length would be only ~60 nm, and the rotational diffusion constant would be ~$10^4\ s^{-1}$, a value well outside any conceivable limits of Figure 3.

The estimation of the intrinsic birefringence of suspended chromatin particles from experimental flow birefringence data and the comparison of this quantity to that calculated for various DNA conformations within the particle have been discussed in detail elsewhere (Harrington, 1979, 1981, 1982). Similar optical modeling techniques have also been applied to the linear dichroism from electrical dichroism studies (Rill & Van Holde, 1974; McGhee et al., 1980, 1983; Houssier et al., 1981; Lee et al., 1981) and from flow dichroism (Tjerneld et al., 1981). As I have noted, theoretical considerations are more straightforward for linear dichroism than for birefringence. Nevertheless, optical modeling results from flow birefringence (Harrington, 1982) based upon the experimental optical anisotropy of DNA have been generally consistent with those from electrical dichroism (Crothers et al., 1978; Wu et al., 1979) at the level of the unfolded nucleosome. Similar results for the 10- and 30-nm chromatin fibers should be similarly valid and should provide an important independent check upon structural models inferred from electrooptical studies and other methods.

Optical parameters obtained from the flow birefringence data of Figure 4 for the 75-mer 30-nm fiber are given in Table I. Values of the optical anisotropy ($g_1 - g_2$) are calculated by using eq 1, and the intrinsic birefringence values are determined by using eq 2 and 3. Since the latter must be calculated explicitly as a function of particle axial ratio (Har-

rington, 1981, 1982), it is obtained here for prolate axial ratios of 3, 5, and 10. Cylindrical inner field shape factors (L_i) are used in eq 3 (Gans, 1912); the differences between these and ellipsoidal shape factors (Peterlin & Stuart, 1939) used previously (Harrington, 1981, 1982; Harrington et al., 1982) are not large, however, and are not significant in terms of other uncertainties in the comprisons made here.

The experimental intrinsic birefringence obtained in this way can be compared to that calculated for helical arrays of chromatosomes stacked in both a face to face and an edge to edge conformation. The basic equation for the intrinsic birefringence of a helix of pitch ρ and radius r is

$$\frac{(\Delta n_{int})_h}{(\Delta n_{int})_s} = -\frac{1}{2}\left[1 - 3\sin^2\left(\tan^{-1}\frac{\rho}{2\pi r}\right)\right] \quad (5)$$

in which Δn_{int} is the intrinsic birefringence and the subscripts h and s refer to the helical and equivalent linear forms, respectively. Equation 5 can be used to calculate the intrinsic birefringence of a solenoidal stack of chromatosomes from the intrinsic birefringence of a "monomeric unit" (including linker DNA) if it is assumed that the stacked chromatosomes form an optical continuum. For present purposes, this assumption is not seriously restrictive since the effective wavelength of the light used, 546 nm (Harrington, 1970c), is long compared to internucleosomal distances for all the models examined here. Δn_{int} values for solenoids of 30-nm diameter and 11-nm pitch are calculated for both face-stacked and edge-stacked models in which the linker DNA is assumed a part of the nucleosomal DNA supercoil, is removed from the 168 bp chromatosome coil at various exit angles but assumed to be straight and rodlike, or is itself supercoiled at the same radius and pitch as core DNA but with a different orientation with respect to the solenoid axis. Because of the inherent limitations in the method, additional variations in the latter model including changing the radius and pitch of the linker supercoil are not reported.

The optical properties of the chromatosomal supercoil are calculated as follows. Let a and b be the major (symmetry) and minor axes, respectively, of cylindrical particles. Using the experimental value $(\Delta n_{int})_s = n_a - n_b = -0.1268$ for linear B-form DNA (Harrington, 1970b; Sarquis & Harrington, 1969), one calculates from eq 5 that $(\Delta n_{int})_{h'} = (n_a - n_b)_{h'} = 0.0610$ for a two-turn chromatosomal helix of $r = 5.5$ nm and $\rho = 2.8$ nm (Harrington, 1982). The primed subscripts indicate that this chromatosome will in turn be used as a monomer in optical models for the solenoid by stacking it in various orientations in a left-handed superhelical array.

The simplest way to stack chromatosomes in a solenoidal array is to position them along a line passing through their major (cylindrical) axis and then to wind this linear array into a left-handed supercoil having the known dimensions of the chromatin fiber. This leads to a radial stacking of the chromatosomes in the solenoid as proposed by McGhee et al. (1980, 1983). If the overall diameter of the fiber is 30 nm and the pitch is 11 nm, the center line would define a helix of $r = 9.5$ nm and $\rho = 11$ nm. From eq 5, the intrinsic birefringence of an optical continuum of chromatosomes having $(\Delta n_{int})_{h'} = (\Delta n_{int})_s = 0.0610$ and stacked wih this geometry is $(\Delta n_{int})_h = -0.0275$. This is somewhat larger than the experimental $\Delta n_{int} = -0.0364$ assuming $r = 5$ for the 75-mer fragment (Table I) but is nevertheless in reasonably close agreement.

The calculated $(\Delta n_{int})_h$ can be decreased by aligning the chromatosomes with their major axes at an angle α with respect to their helical trajectory. The pitch angle of a helix is $\cot\beta = 2\pi r/\rho$; for $r = 9.5$ nm and $\rho = 11$ nm, $\beta = 10.4°$. For $\alpha = \beta$ (chromatosomes stacked such that their faces lie parallel to the solenoid axis), $(\Delta n_{int})_s = n_1(a) - [n_b + n_2(b)]/2 = 0.0916$ using eq 15a,b of Harrington (1981) and averaging as required by the effective cylindrical symmetry of the fiber; eq 5 for this case predicts that $(\Delta n_{int})_h = -0.0413$ for the solenoid. Exact agreement with the experimental Δn_{int} occurs at $\alpha = 6.6°$, the pitch angle of a helix of $r = 15$ nm and $\rho = 11$ nm, but this level of agreement is probably fortuitous since this stacking model does not include contributions from the linker DNA except for the special case in which the linker follows a helical trajectory identical with that in the chromatosome itself.

An alternative model for chromatosome stacking has been proposed (Suau et al., 1979) in which the chromatosome faces are approximately normal to the solenoid axis. This corresponds generally to a face to face stacking longitudinally along the solenoid axis. We may approximate this model by aligning the chromatosomes edge to edge along a helical trajectory. For this case, $(\Delta n_{int})_s = n_b - (n_a + n_b)/2$ as required by symmetry, and $(\Delta n_{int})_h = 0.0317$ from eq 5. This positive value for the birefringence is clearly at variance with experiment, in agreement with similar conclusions reached by McGhee et al. (1980, 1983) from analysis of electric dichroism data. The discrepancy is reduced if the chromatosome faces lie at a small angle, $\xi = 90° - \alpha$, with respect to the helical trajectory. For $\alpha = 6.6°$, $(\Delta n_{int})_s = n_1(a) - [(n_b + n_2(b)]/2 = 0.0038$ and $(\Delta n_{int})_h = -0.0017$, and for $\alpha = 10.4°$, $(\Delta n_{int})_h = -0.0097$. In all cases, however, agreement is far less satisfactory than for the radially stacked edge to edge model. Furthermore, the assumptions in this case with respect to linker DNA contributions to the calculated birefringence are much less satisfactory.

The effects of the linker DNA on the optical models can be investigated by allowing the linker regions to assume certain configurations and including these explicitly in the optical modeling calculations. The simplest case represents the linker regions as straight rodlike segments at various orientations with respect to the stacked chromatosomes. Chicken erythrocyte chromatin has about 44 bp of linker DNA per chromatosome. If this is in the B form, its contour length is about 15 nm. General methods for estimating Δn_{int} of a chromatosome with straight linkers extending symmetrically on either side have been given previously (Harrington, 1982). The birefringence can be obtained as a function of two DNA exit angles: a "dihedral" angle (ϕ) and a "core twist" angle (θ) [see, e.g., Figure 11 of this work or model C, Figure 7 of Harrington (1982)]. By use of these methods, $(\Delta n_{int})_s$ has been obtained by computer for all combinations of ϕ and θ between 0° and 90°, respectively. In these calculations, $(\Delta n_{int})_s = n_a - (n_b + n_{b'})/2$ where a is the longitudinal axis of the linker and b and b' are respectively the other two coordinate axes. This places the linker axis a roughly along a helical trace defining the solenoid pitch and gives equal weight to the chromatosome major and minor axes in the effective cylindrical symmetry of the solenoid. The dihedral angle $\phi \pm \beta$, where β is the actual pitch of the helical trajectory in the solenoid, therefore defines the tilt of the linkers in the direction normal to the solenoid axis, and the twist θ defines the cant of the linkers away from the chromatosome faces. Results are shown in Figure 8 in which the region of ±10% agreement with experiment ($r = 5$) is shaded. Although the model is also grossly oversimplified, the results include structurally plausible conformations and suggest as in the linkerless models discussed above that conformations near $\theta = 90°$ (radially edge-stacked conformations if the linkers follow roughly a helical trajectory through the

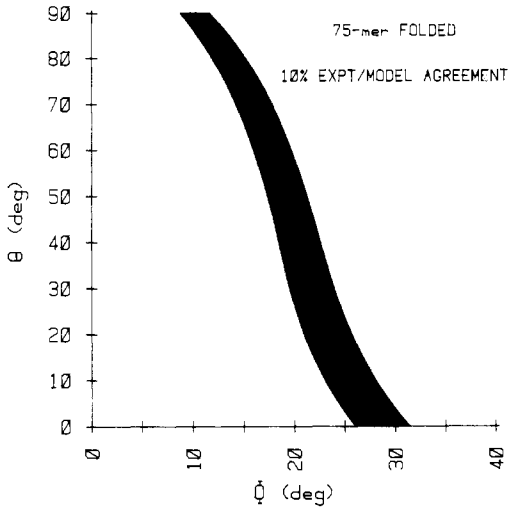

FIGURE 8: Experimental consistency plot at the ±10% level for solenoid models of the condensed 75-mer chromatin fiber showing the effects of linker DNA orientation with the assumption that the linker DNA is straight and rodlike. The angle θ is the core twist or out of plane tilt, and ϕ is the dihedral angle of the linker DNA with respect to the chromatosomes. The arrangement of linker DNA and chromatosomes along a solenoidal trajectory therefore corresponds to that shown in Figure 11.

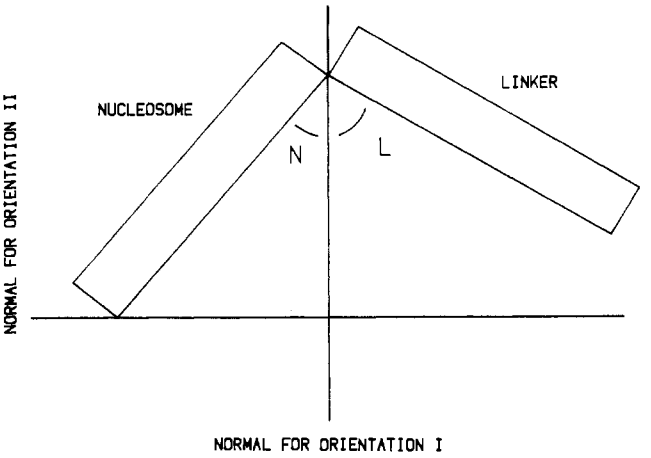

FIGURE 9: Definition of angular orientation parameters N and L for solenoid models of the condensed 75-mer chromatin fiber in which both nucleosomal and linker DNA are modeled as supercoils. Axes (normals) are with respect to the solenoidal trajectory of the chromatosome-linker array.

fiber) with small values of ϕ are acceptable.

More sophisticated models may also be investigated in which the linker regions are also allowed to form a supercoil. For simplicity, this supercoil is taken to have the same diameter and pitch as the nucleosomal DNA itself, but with the faces of the linker supercoils oriented at a different angle. The monomer for this model is shown schematically in Figure 9. Two principal orientations with respect to the chromatin fiber axis are shown. Orientation I is that in which a plane normal to the helical trajectory of the polynucleosomal array through the solenoid passes between the nucleosomal and linker supercoils (modeled here as disks) and includes the single unique contiguous point; the cants of the chromatosomal and linker disks with respect to this plane are N and L, respectively. Orientation II simply rotates this chromatosome-linker array by 90°. In both cases, the effective cylindrical symmetry of the array along the helical trace is maintained by averaging the radial refractive index components of this cylindrical array over the two orthogonal directions normal to the overall solenoid axis.

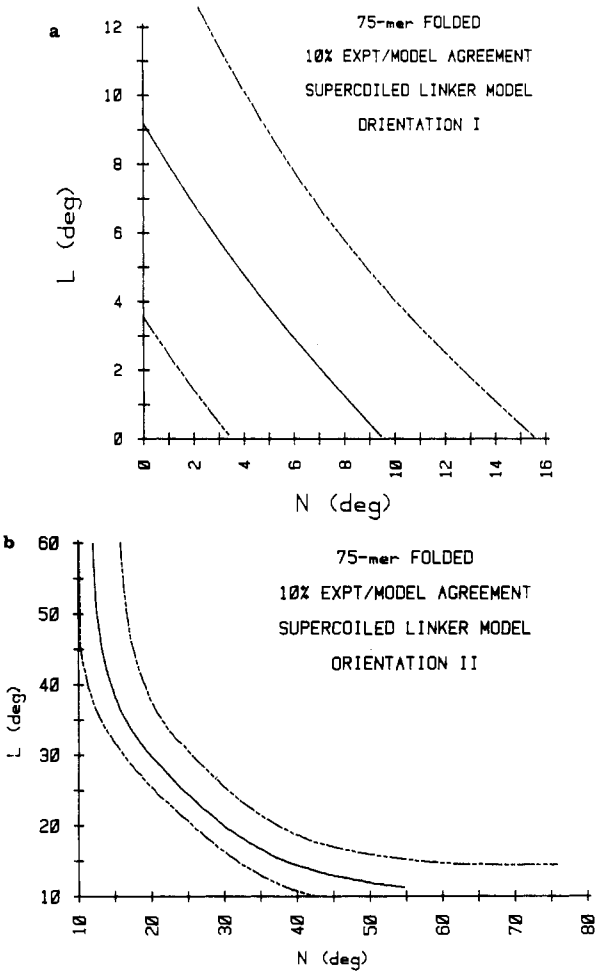

FIGURE 10: Experimental consistency plot at the ±10% level for solenoid models of the condensed 75-mer chromatin fiber in which both nucleosomal DNA and linker DNA are modeled as supercoils. Angular variables and orientations are as given in Figure 9. (a) Orientation I; (b) orientation II.

Model building suggests that orientation I leads to a reasonable structure for the 30-nm fiber which is very similar to the edge-stacked, radial orientation of chromatosomes suggested by McGhee et al. (1980, 1983). The optical properties of the split double-supercoil monomeric structure were calculated as a function of the dihedral angles N and L by using methods described in detail elsewhere (Harrington, 1981). The solenoid anisotropy was then obtained by using eq 5 with $(\Delta n_{int})_s = n_1 - (n_b + n_2)/2$ where $n_b = 1.6080$ is the radial refractive index component of the nucleosome or linker supercoil and n_2 and n_1 are the components along and at right angles to the orientation I normal axis of Figure 9, respectively. The effect upon solenoid anisotropy for various values of chromatosome or linker r and ρ values is not large: $(\Delta n_{int})_{h'}$ for these supercoils varies from 0.063 to 0.055 for $r = 7.5$ and $\rho = 2.0$ nm and for $r = 4.0$ and $\rho = 5.5$ nm, respectively. Although these differences are significant, their effects upon the optical modeling are relatively minor in comparison with N and L, the principal determinants of monomer anisotropy.

The results of the optical model calculations for orientation I are shown in Figure 10a. The loci of N and L values which lead to the experimental Δn_{int} for $r = 5$ are shown as a solid curve with dashed lines representing arbitrary discrepancy limits of ±10%. Values of N near the solenoid pitch angle of 6–10° correspond roughly (in terms of the presumed cylindrical symmetry of the helical polynucleosome-linker array) to chromatosome orientations in which the faces are approx-

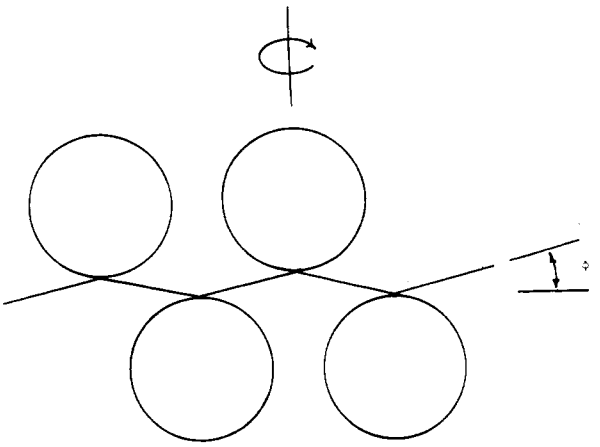

FIGURE 11: Schematic representation for the low-salt (unfolded) chromatin fiber (chromatosome disks viewed down the cylindrical axes). The angle θ is the out of plane chromatosome core twist with respect to the plane defined by the linker DNA ($\theta = 0$ when the disks lie in the plane), and the angle ϕ is the dihedral angle (or exit angle) of the linker DNA (assumed straight and rodlike) with respect to the internucleosomal axis.

imately parallel to the solenoid axis. The resulting family of solenoids also seems to derive naturally from structural model building and is conceptually similar to the McGhee et al. (1980, 1983) structures deduced from analysis of limiting electric dichroism data.

Orientation II, the orthogonal orientation of the split supercoil monomer in the helical trace of the solenoid, would lead to face-stacked helical polynucleosomal arrays for small N and L but would become more ambiguous as N and L become larger, finally approaching orientation I as a limit. Optical properties of the solenoid for this case are calculated as described above with the monomer refractive index components n_2 and n_1 interchanged. Results are shown in Figure 10b. Again, the dashed lines represent disagreement limits of ±10% between the experimental $r = 5$ and calculated Δn_{int} values. The curves are shown over that range of N and L for which these limits can exist.

The helical trace of the solenoid is constrained by fiber geometry and total number of chromatosomes to be relatively shallow. Hence, orientation II with N and L small corresponds to a face-stacked chromatosome orientation. From Figure 10b, conformers with N and L simultaneously $<\sim 20$–$30°$ are highly improbable. A face-stacked orientation (N small) with linker supercoil faces aligned nearly along the solenoid axis (L large) might be possible, but this would generally lead to an excessively large overall solenoid pitch. These considerations, along with the fact that probable optical conformers are so highly constrained in Figure 10b, suggest that orientation II is relatively unlikely conformation. This is particularly true for those angular variants leading to largely face-stacked orientations of chromatosomes in the solenoid.

10-nm Fiber. The experimental birefringence data on the low-salt form of the 10-mer fiber are used for optical model analysis because, as noted, larger fragments show evidence of appreciable chain flexibility. Experimental results are shown in Table I. Since the extinction angle data suggest an almost complete unfolding of the solenoid, a linear arrangement of chromatosomes such as is shown schematically in Figure 11 seems a reasonable model. Linker regions are shown as straight for conceptual simplicity and by analogy with free DNA in solution (Harrington, 1982). Optical calculations applicable to this model have been described (Harrington, 1982), and the same angular conventions are used here: ϕ is the dihedral or exit angle of the linker DNA from the chromatosome, and θ is the twist angle of the chromatosome faces with respect to the plane of the drawing. The optical properties of this model are unchanged if adjacent chromatosomes are on the same side of the linker regions instead of alternating opposite as shown. This is a consequence of the cylindrical symmetry of measurement in the flow birefringence method.

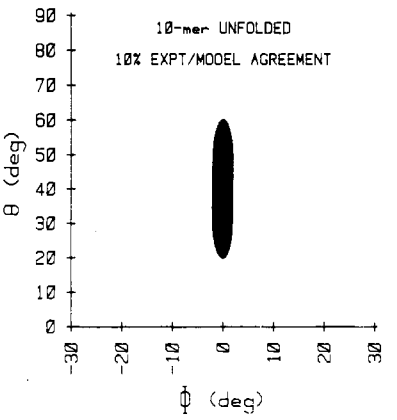

FIGURE 12: Experimental consistency plot at the ±10% level for the low-salt (unfolded) 10-mer chromatin fiber. The angular variables θ and ϕ are as defined in Figure 11.

Results of computer modeling of the intrinsic birefringence are given in Figure 12. The dark region corresponds to ±10% agreement with the experimental intrinsic birefringence assuming an axial ratio $p = 10$. The region of theoretical agreement in this case is quite restricted: θ can range from $\sim 20°$ to $60°$, but ϕ is restricted to a narrow range of $\sim \pm 5°$. Thus, the unfolded fiber appears to be quite extended although it is not certain whether all or part of this might be due to tensional stresses on the fiber resulting from the hydrodynamic orientation. In any event, these results are certainly in agreement with the electric dichroism results of McGhee et al. (1980, 1983) and provide an independent justification of their model in which both chromatosome faces and linkers are aligned along the direction of the orienting electric field with a maximum permissible tilt (the θ value used in this report) of $\sim 20°$. This level of agreement is significant in that electric orientation and hydrodynamic orientation are physically different processes and the two experiments are done under quite different limiting conditions. In addition, the internal architecture of the fiber undoubtedly permits appreciable flexibility.

The anomalously high level of kinetic flexibility observed in the 10-nm chain relative to pure, native DNA at high salt (Figure 6) may be associated with the linker region or possibly even with the exit points of the DNA from the chromatosomal region. This would suggest that interactions of core histones with chromatin DNA are not confined exclusively to the chromatosome region. As suggested by McGhee et al. (1980), this flexibility may serve a function since any correlation between the 10-nm fiber and the structure of the condensed 30-nm fiber is thereby reduced.

Other Optical–Hydrodynamic Studies on Chromatin. There are some areas of disagreement between the results shown in Figures 2 and certain other linear flow dichroism studies. These are chiefly in the sign of the optical effect at low ionic strength. Makarov et al. (1983) have reported a positive dichroism in whole calf thymus chromatin between 2 and 100 mM Na^+ (R between ~ 1 and 22 in Figure 2) with the sign becoming negative again at higher ionic strengths. They interpret this sign change as a structural reorientation of the chromatosome faces from essentially a parallel orientation along the open fiber axis to a more orthogonal one.

Although their experimental dichroism curve below ~100 mM is quite similar to Figure 2, I do not believe that the two studies are directly comparable. First, the positive birefringence observed here derives from the form effect; this effect is believed to be much smaller for linear dichroism (Fredericq & Houssier, 1973). More seriously, the results of Mararov et al. (1973) may not have been obtained under steady-state conditions since they used a unique, pulsed linear flow apparatus in their studies. The longest relaxation time for free solvent shear decay in a parallel plate device may be as long as several tenths of a second (Lamb, 1932; Thompson & Gill, 1967), and the optical properties of oscillatory flow systems are known to be greatly different from corresponding steady-state values (Thompson & Gill, 1967; Thurston & Schrag, 1967). Finally, artifactual differences among chromatins from different sources are always possible.

More serious discrepancies appear to exist between the present results and those reported by Norden and co-workers (Tjerneld et al., 1982; Matsuoka et al., 1984). These authors obtained positive linear dichroism for certain chromatin systems at low ionic strengths using flow orientation in a Wada & Kozawa (1964) cell at 1800–2000-s^{-1} shear. This flow cell has been criticized both for its relatively short optical path length and for its propensity toward Taylor instability at velocity gradients above ~500 s^{-1} (Lee & Davidson, 1968). Furthermore, the dichroism data were obtained under relatively high-shear and concentration conditions whereas the present results represent the zero limit of both variables. It is difficult to see how nonlaminar flow conditions could lead to a sign inversion in the optical properties, however, and I suspect that the reasons for the observed discrepancies lie in the different chromatin preparations used or in their state at the time of measurement. Clearly, additional study will be required to resolve these questions.

Conclusions

I have used hydrodynamic orientation and experimental determination of birefringence to deduce the conformation of DNA in the unfolded 10-nm and folded 30-nm fibers of chromatin. The results suggest a relatively flexible (relative to pure DNA) "beads on a string" model for the open fiber and an edge to edge stacked array of chromatosomes for the condensed system. The results are also consistent with the radially stacked model of McGhee et al. (1980, 1983) and generally corroborate the results of these electric dichroism studies. Since these methods are physically distinct and involve different sources of potential error, the results presented here represent an important confirmation of the McGhee et al. (1980, 1983) structural models for chromatin in solution.

Flow birefringence as a method to characterize systems such as those described here is advantageous in that it is now possible to measure very precisely both small birefringence and weak orientation under dilute solution conditions. Hydrodynamic orientation of anisometric particles is now quite well understood and does not suffer from the uncertainties still remaining in our understanding of polyelectrolyte effects associated with electrical orientation. Further, measurements reported here are made in the limit of zero perturbation by the orienting (hydrodynamic) field rather than in the infinite field limit of electric dichroism. On the other hand, the optical theory of birefringence is much less satisfactory than that of dichroism, especially since the form effect is relatively large in birefringence and small in dichroism. In this work, modeling results are based upon the *experimental* anisotropy of pure DNA, and no attempt is made to treat this quantity theoretically. Since the intrinsic and form birefringence components appear to model similarly (Harrington, 1967, 1979, 1982) and the large intrinsic optical anisotropy of DNA greatly exceeds that of the protein components of chromatin (Harrington, 1979, 1981, 1982), there seems to be no a priori reason to suspect the present methods on theoretical grounds.

In spite of this, the models proposed here and elsewhere cannot be taken too literally, but rather represent constraints upon the various possible models for chromatin structure that can be envisioned. There is no uniqueness in conclusions drawn from optical modeling—only consistence with certain structures and inconsistence with others. Nevertheless, these methods can assign relative probabilities to particular structures. Since the structures represented as highly probable by the present modeling techniques are reasonable, and since these same structures are assigned high probability by other, independent biophysical methods, I feed that these now represent good working hypotheses for the further examination of structure–function relationships in chromatin.

Acknowledgments

I am particularly indebted to Professor J. D. McGhee for initially suggesting and encouraging this work and for providing chromatin samples for comparative study. Acknowledgments are also due to Dr. Walter Baase, Dr. Eliot Charney, and Professors John Schellman and Donald M. Crothers for helpful comments. The technical assistance of Kim Cairney Spears in the preparation of samples and in the acquisition of much of the data reported here is also gratefully acknowledged.

References

Azorin, F., Martinez, A. B., & Suberana, J. A. (1980) *Int. J. Biol. Macromol. 2*, 81–92.

Baldwin, J. P., Carpenter, B. G., Crespi, H., Hancock, R., Stevens, R. M., Simpson, J. K., Bradbury, E. M., & Ibel, K. (1978) *J. Appl. Crystallogr. 11*, 484–486.

Barrett, T. W., & Harrington, R. E. (1977) *Biopolymers 16*, 2167–2188.

Colson, P., Houssier, C., & Fredericq, E. (1974) *Biochim. Biophys. Acta 340*, 244–261.

Crothers, D. M., Dattagupta, N., Hogan, M., Klevan, L., & Lee, K. S. (1978) *Biochemistry 17*, 4525–4550.

Edmonds-Alt, X., Houssier, C., & Fredericq, E. (1979) *Biophys. Chem. 10*, 27–39.

Finch, J. T., & Klug, A. (1976) *Proc. Natl. Acad. Sci. U.S.A. 73*, 1897–1901.

Finch, J. T., Lutter, L. C., Rhodes, D., Brown, R. S., Rushton, B., Levitt, M., & Klug, A. (1977) *Nature (London) 269*, 29–36.

Fredericq, E., & Houssier, C. (1973) in *Electric Dichroism and Electric Birefringence*, Chapter 1, pp 41–43, Clarendon Press, Oxford.

Gans, R. (1912) *Ann. Phys. (Leipzig) 37*, 881–900.

Gill, S. J., & Thompson, D. S. (1967) *Proc. Natl. Acad. Sci. U.S.A. 57*, 562–566.

Harrington, R. E. (1967) *Encycl. Polym. Sci. Technol. 7*, 100–179.

Harrington, R. E. (1970a) *Biopolymers 9*, 159–193.

Harrington, R. E. (1970b) *J. Am. Chem. Soc. 92*, 6957–6964.

Harrington, R. E. (1970c) *Biopolymers 9*, 141–158.

Harrington, R. E. (1979) in *Chromatin Structure and Function, Part A* (Nicolini, C., Ed.) pp 167–185, Plenum Press, New York.

Harrington, R. E. (1981) *Biopolymers 20*, 719–752.

Harrington, R. E. (1982) *Biochemistry 21*, 1177–1186.

Harrington, R. E. (1983) *Biophys. J. 41*, 43a.
Harrington, R. E., & Martin, K. V. (1969) *Biopolymers 7*, 627–648.
Harrington, R. E., Uberbacher, E. C., & Bunick, G. J. (1982) *Nucleic Acids Res. 10*, 5695–5709.
Houssier, C. (1981) *NATO Adv. Study Inst. Ser, Ser. B 64*, 363–398.
Houssier, C., & Fredericq, E. (1966) *Biochim. Biophys. Acta 120*, 113–120.
Houssier, C., & Tricot, M. (1979) in *Electro-Optics and Dielectrics of Macromolecules and Colloids* (Jennings, B. R., Ed.) pp 247–257, Plenum Press, New York.
Houssier, C., Hacha, R., DePauw-Gillet, M. C., Pieczynski, J. L., & Fredericq, E. (1981a) *Int. J. Biol. Macromol. 3*, 59–62.
Houssier, C., Lasters, I., Muyldermans, S., & Wyns, L. (1981b) *Nucleic Acids Res. 9*, 5763–5784.
Kasha, M., Elbayouni, M., & Rhodes, W. (1961) *J. Chem. Phys. 58*, 917–923.
Kornberg, R. (1977) *Annu. Rev. Biochem. 46*, 931–954.
Lamb, H. (1932) in *Hydrodynamics* 6th ed., p 590, Dover Publications, New York.
Lee, C. S., & Davidson, N. (1968) *Biopolymers 6*, 531–550.
Lee, K. S., Mandelkern, M., & Crothers, D. M. (1981) *Biochemistry 20*, 1438–1445.
Makarov, V. L., Dimitrov, S. I., & Petrov, P. T. (1983) *Eur. J. Biochem. 133*, 491–497.
Marion, C., & Roux, B. (1978) *Nucleic Acids Res. 5*, 4431–4449.
Matsuoka, Y., Nielsen, P. E., & Norden, B. J. F. (1984) *FEBS Lett. 169*, 309–312.
McGhee, J. D., & Felsenfeld, G. (1980) *Annu. Rev. Biochem. 49*, 1115–1156.
McGhee, J. D., Rau, D. C., Charney, E., & Felsenfeld, G. (1980) *Cell (Cambridge, Mass.) 22*, 87–96.
McGhee, J. D., Nickol, J. M., Felsenfeld, G., & Rau, D. C. (1983) *Cell (Cambridge, Mass.) 33*, 831–841.
Mirzabekov, A. D. (1980) *Q. Rev. Biophys. 13*, 255–295.
Oriel, P. J., & Schellman, J. A. (1966) *Biopolymers 4*, 469–494.
Peterlin, A., & Stuart, H. A. (1939) *Z. Phys. 113*, 663–686.
Richmond, T. J., Finch, J. T., Rushton, B., Rhodes, D., & Klug, A. (1984) *Nature (London) 311*, 532–537.
Rill, R., & Van Holde, K. E. (1974) *J. Mol. Biol. 83*, 459–471.
Ris, H., & Korenberg, J. (1979) in *Cell Biology* (Prescott, D. M., & Goldstein, L., Eds.) pp 267–331, Academic Press, New York.
Roux, B., Marion, C., & Bernengo, J. C. (1979) in *Electro-Optics and Dielectrics of Macromolecules and Colloids* (Jennings, B. R., Ed.) pp 163–173, Plenum Press, New York.
Ruiz-Carillo, A., Puigdomenech, P., Elder, G., & Lurz, R. (1980) *Biochemistry 19*, 2544–2554.
Sarquis, J. L., & Harrington, R. E. (1969) *J. Phys. Chem. 73*, 1685–1694.
Scheraga, H. A. (1951) *J. Chem. Phys. 19*, 983–984.
Scheraga, H. A., & Signer, R. (1960) in *Physical Methods of Organic Chemistry* (Weissberger, A., Ed.) Vol. I, Part III, Chapter 33, Interscience, New York.
Shinde, H., McGhee, J. D., & Cohen, J. S. (1980) *Biopolymers 19*, 523–538.
Simpson, R. (1978) *Biochemistry 17*, 5524–5531.
Stellwagen, N. C. (1981) *Biopolymers 20*, 399–434.
Suau, P., Bradbury, E. M., & Baldwin, J. P. (1979) *Eur. J. Biochem. 97*, 593–602.
Taylor, E. W., & Cramer, W. (1963) *Biophys. J. 3*, 127–141.
Thoma, F., Koller, T., & Klug, A. (1979) *J. Cell Biol. 83*, 403–427.
Thompson, D. S., & Gill, S. J. (1967) *J. Chem. Phys. 47*, 5008–5017 (Appendix I).
Thurston, G. B., & Schrag, J. L. (1967) *J. Chem. Phys. 45*, 3373–3380.
Tirado, M. M., & Garcia de la Torre, J. (1980) *J. Chem. Phys. 73*, 1986–1993.
Tjerneld, F., Norden, B. J. F., & Wallin, H. (1982) *Biopolymers 21*, 343–358.
Wada, A., & Kozawa, S. (1964) *J. Polym. Sci., Part A-2*, 853–860.
Wu, H. M., Dattagupta, N., Hogan, M., & Crothers, D. M. (1979) *Biochemistry 18*, 3960–3965.